On the ionospheric source region of cold ion outflow

K. Li,[1,2,3] S. Haaland,[2,4] A. Eriksson,[5] M. André,[5] E. Engwall,[5] Y. Wei,[2] E. A. Kronberg,[2] M. Fränz,[2] P. W. Daly,[2] H. Zhao,[6] and Q. Y. Ren[6]

Received 25 July 2012; revised 9 August 2012; accepted 9 August 2012; published 20 September 2012.

[1] Recent studies have shown that low energy ions constitute a significant part of the total ion population in the Earth's magnetosphere. In this study, we have used a comprehensive data set with measurements of cold (total energy less than 70 eV) ion velocity and density to determine their source. This data set is derived from Cluster satellite measurements combined with solar wind and interplanetary magnetic field measurements and geomagnetic indices. By using the guiding center equation of motion, we were able to calculate the trajectories and thus determine the source region of the cold ions. Our results show that the polar cap region is the primary source for cold ions. We also found that the expansion and contraction of the polar cap as a consequence of changes in solar wind parameters were correlated with the source region size and intensity of the cold ion outflow. Elevated outflow fluxes near the nightside auroral zone and the dayside cusps during disturbed conditions suggest that energy and particle precipitation from the magnetosphere or directly from the solar wind can enhance the outflow of cold ions from the ionosphere. **Citation:** Li, K., et al. (2012), On the ionospheric source region of cold ion outflow, *Geophys. Res. Lett.*, *39*, L18102, doi:10.1029/2012GL053297.

1. Introduction

[2] Every day, the Earth loses mass through ions escaping from polar ionosphere. The importance of this outflow as a supplier of plasma to the terrestrial magnetosphere, ionosphere-magnetosphere coupling, and even the evolution of atmosphere itself [*Moore and Horwitz*, 2007; *Wei et al.*, 2012], has been recognized for decades, and there are suggestions that the ionosphere alone is a sufficient source to account for the observed magnetospheric plasma population [*Chappell et al.*, 1987]. Most of the knowledge come from in-situ observations made by particle detectors onboard spacecraft, and thus the earlier data sets were often dominated by ions with energy above tens of eV because a sunlit spacecraft is often positively charged to several tens of Volts.

[3] The cold ions, the very low energy part of the plasma population (energies below the equivalent spacecraft potential energy), exhibit some surprising features and even challenge the current picture about ion outflow. For example, cold ions can co-exist with hot ions in the plasma sheet [*Seki et al.*, 2003]; the escape rate of cold ions could be one order higher than that of hot ions on Earth [*Engwall et al.*, 2009a; *Peterson et al.*, 2006], and also on Mars and Venus [*Dubinin et al.*, 2011]. What has become clear is that it is time to renew the picture of ion outflow by investigating and then integrating the nature of cold ions to the whole picture [*André and Cully*, 2012].

[4] Earlier studies [e.g., *Yau and André*, 1997; *Moore and Horwitz*, 2007], have shown that there are several important source regions for the outflow; the polar wind, the ion cleft and the auroral region. In addition, plasmaspheric plumes providing cold plasma sometimes also dominate the dayside magnetosphere [*André and Cully*, 2012].

[5] Due to spacecraft charging effects, it has been difficult to measure the cold ions. And until recently, the cold plasma population was regarded as "hidden" [*Chappell et al.*, 1987]. For this reason, quantitative studies about the source region of cold ion outflow as well as its response to solar wind, the interplanetary magnetic field (IMF) and geomagnetic activity have been rare.

[6] Recent advances in instrumentation and methodology, combined with more comprehensive measurements from Cluster and auxiliary data have provided far better opportunities to assess the role of the cold ions. In particular, it is now possible to obtain very accurate measurements of density [*Lybekk et al.*, 2012], and outflow velocity [*Engwall et al.*, 2009b, 2009a] of cold ions. Cluster also provides more accurate and more comprehensive convection measurements [*Haaland et al.*, 2008] than earlier missions.

[7] In this work, we utilize these advantages to identify the primary source region of cold ionospheric outflow, and investigate how this source region changes with changing solar wind and geomagnetic conditions.

2. Cold Ion Outflow Measurements

[8] The data basis for this study was compiled by *Engwall et al.* [2009b, 2009a] and later also used by *Haaland et al.* [2012] to study the fate of cold ions of ionospheric origin. The data set is based on a combination of spacecraft potential, wake electric field and convection measurements to calculate the density and velocity of the outflowing cold ions. The measurements are obtained from the Electric Field and Wave instrument (EFW) [see *Gustafsson et al.*, 2001], the electron drift instrument (EDI) [see *Paschmann et al.*, 2001], and the

[1]State Key Laboratory of Space Weather, Center for Space Science and Applied Research, Chinese Academy of Sciences, Beijing, China.
[2]Max-Planck Institute for Solar System Research, Katlenburg-Lindau, Germany.
[3]Graduate University of Chinese Academy of Sciences, Beijing, China.
[4]Department of Physics and Technology, University of Bergen, Bergen, Norway.
[5]Swedish Institute of Space Physics, Uppsala, Sweden.
[6]Beijing Institute of Spacecraft Environment Engineering, Beijing, China.

Corresponding author: S. Haaland, Max-Planck Institute for Solar System Research, Max-Planck-Strasse 2, Katlenburg-Lindau DE-37191, Germany. (stein.haaland@issi.unibe.ch; likun@mps.mpg.de)

0094-8276/12/2012GL053297

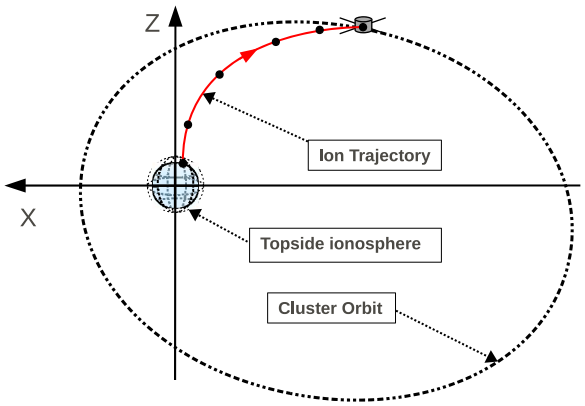

Figure 1. Schematic diagram showing the tracing technique. For every cold ion recorded, its acceleration along the magnetic field line and convection velocity can be calculated to trace the cold ion along its trajectory, all the way back to topside ionosphere. The final landing point in the ionosphere is defined as the source region.

fluxgate magnetometer (FGM) [see *Balogh et al.*, 1997]. The EDI instrument, which relies on the detection of an artificially emitted electron beam, does not have a fixed time resolution, but provides a signal each time the beam hits the sensor. One such hit is used to determine the convective electric field. The concurrent spacecraft potential and the spin averaged E-field from EFW are then used to calculate the electron density and parallel velocity, respectively.

[9] In the cold tenuous plasma of the polar cap and lobe regions, the spacecraft potential, V_{sc}, typically exceeds the equivalent bulk kinetic energy (E_k) of the ions, which on the other hand is larger than the thermal energy of the ions. Under such conditions, a large wake forms behind the spacecraft [*Eriksson et al.*, 2006]. By combining data from EFW and EDI, this wake can be detected and used to derive the full velocity vector of the flowing ions [*Engwall et al.*, 2009b, 2009a].

[10] It is not possible to distinguish between different ion species with this method. Since the velocity determination relies on the identification of this wake, for the same velocity, the heavier ions with higher kinetic energy can penetrate into the wake. Thus the method is typically more sensitive to protons than to heavier ions. In the following, we therefore assume that the ions are H+, although heavy ion outflow can be significant, in particular during disturbed magnetospheric conditions.

[11] The cold plasma density can be derived from the spacecraft potential by noting that a functional dependence between ambient electron density and the spacecraft potential exists [e.g., *Pedersen et al.*, 2001]. In the polar cap and lobe regions, the spacecraft potential can reach values up to 60–70 V. When referring to "cold ions", we therefore mean ions with kinetic energies up to 70 eV and typical thermal energies of a few eV.

[12] For a more detailed description of the methodology, as well as an assessment of its accuracy, we refer to the original publication by *Engwall et al.* [2009a].

[13] In addition to cold density and velocity, we also make use of the magnetic field as well as auxiliary parameters such as solar wind measurements and geomagnetic activity indices to study correlations. In total, we have approximately 180 000 measurements, taken in the period July to November for each of the years 2001–2005.

3. Tracing Methodology

[14] With knowledge about spacecraft position as well as parallel and perpendicular velocity of the cold ions, we can trace the ions back to their origin in the ionosphere (see Figure 1), using the guiding center equations of motion [*Northrop*, 1963]. Assuming conserved flux along a magnetic field line, we can also determine the flux in the source region.

[15] For our purpose, the first order guiding center equation of motion given in *Northrop* [1963] can be somewhat simplified. First, in the regions considered here, i.e., the polar caps and lobe regions at 4–19 Re altitude, the magnetic field lines can be assumed to be equipotential. Acceleration due to parallel electric fields is therefore not relevant, but the convection enters the equation of motion. Since we do not know the magnetic moments of the ions, it is not possible to assess acceleration due to mirror forces. The parallel velocity at low altitudes may thus be overestimated and travel time underestimated in our calculations. Since the ionospheric convection is typically a few 100 m/s, this will not have any significant impact on the footpoint, however. The total parallel acceleration of the particles therefore reduces to

$$a = \vec{V_E} \cdot \frac{d\hat{b}}{dt} + g_{\parallel}, \tag{1}$$

where $\vec{V_E}$ is the convection velocity, $\hat{b}$ is a unit vector along the magnetic field, and $g_{\parallel}$ is the component of gravity along the magnetic field.

[16] The first term of equation (1) represents the centrifugal acceleration [*Cladis*, 1986]. *Nilsson et al.* [2010] investigated the influence of the centrifugal acceleration on the cold ions in the same data set as we use, and found typical values of a few m/s^2. In our calculations, we have used magnetic field values from the TS05 [*Tsyganenko and Sitnov*, 2005] magnetic field model. The model has been properly parameterized with the prevailing solar wind, IMF and activity indices. At a given point along the ion's trajectory, the convection velocity, $\vec{V_E}$, is derived from EDI measurements, and is scaled by the corresponding model magnetic field, $\vec{B}$:

$$\vec{V_E} = \left| \vec{V_{E,sc}} \right| \sqrt{|\vec{B_{sc}}|/|\vec{B}|}\,(\vec{B}\cdot\nabla)\vec{B}/|(\vec{B}\cdot\nabla)\vec{B}| \tag{2}$$

where $\vec{V_{E,sc}}$ and $\vec{B_{sc}}$ are convection velocity and magnetic field measured at the spacecraft position, respectively.

[17] Figure 2 shows a typical example of calculated values along the trajectory of an ion starting out at 1000 km altitude in the southern polar cap ionosphere and detected by Cluster at about 9 Re altitude in the southern hemisphere lobe.

[18] Close to Earth, the magnetic field is strong (approximately 37 000 nT), with a low convection velocity. As a result, the centrifugal acceleration is still negligible, and the equation of motion is still dominated by gravity. Above approximately 1.5 Re altitude, the centrifugal acceleration starts to dominate, and the ion is effectively accelerated

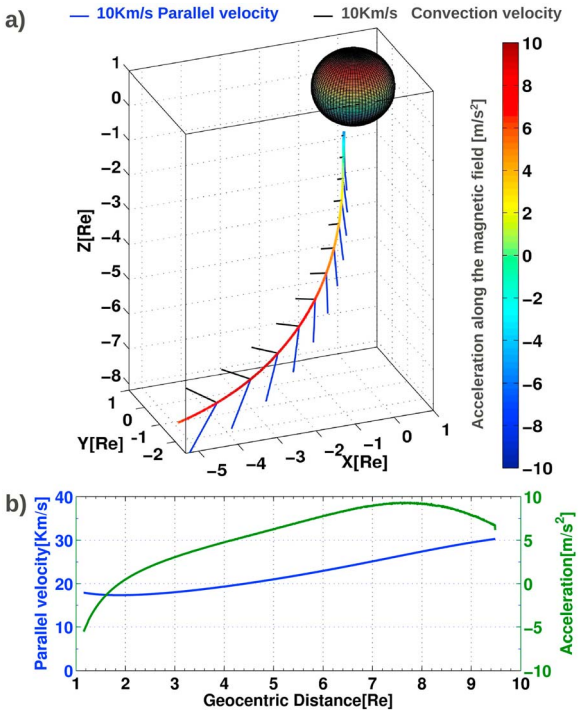

Figure 2. Example calculations with key parameters and trajectory of a cold ion, observed by Cluster, located at position [−5.33, −2.17, −7.55] Re_{GSM} in the southern hemisphere. Travel time from the topside ionosphere at 1000 km altitude to Cluster was found to be 40 min 40 sec. B_{IMF} was [3.3, −5.2, 0.0] nT_{GSM} and the solar wind dynamic pressure was 2.6 nPa for this case. (a) Calculated trajectory of the cold ion, with colors indicating the acceleration along the magnetic field. The convection and parallel velocities are also shown as black and blue vectors, respectively. (b) Acceleration and parallel velocity shown as function of altitude.

outwards from the ionosphere and into the magnetosphere. For this particular example, the maximum acceleration is reached around 7.5 Re altitude. Further tailward, the magnetic field tends to straighten out, and the effect of centrifugal acceleration starts to subside, but still remains positive. The ion will therefore continue to be accelerated as it travels outwards through the lobes.

4. Source Regions

[19] Approximately 104 000 observations could be traced back to the ionosphere using the above method. (For the remaining cases, the tracing failed or suggested a source region outside the ionosphere.) From those 104 000 cases, 58 418 cases were traced back to the northern hemisphere and 45 564 cases were traced back to the southern hemisphere.

[20] Figure 3 shows maps of the source regions for three different levels of geomagnetic activity for the northern and southern hemisphere respectively. Each pixel in these maps represents the average flux from all measurements within a roughly 65 000 km^2 source area at 1000 km altitude. An altitude corrected geomagnetic coordinate system (AACGM) [see *Baker and Wing*, 1989] has been used.

[21] As a measure of geomagnetic activity, we have chosen to use the Disturbed Storm Time (Dst) index. This 1 hour index is a proxy for the total energy in the Earth's ring current, and is mainly modulated by geomagnetic storms - i.e., processes with time scales of hours to days. The long transport times involved in cold ion outflow combined with the focus on global activity makes this index more suitable than e.g., the Auroral Electrojet (AE) index used to characterize short time, localized phenomena such as auroral activity and bursty bulk flow transport in the magnetotail. However, there is often a strong mutual correlation between the various activity indices, and also solar wind parameters [e.g., *Förster et al.*, 2007]. As demonstrated in Table 1, both the AE and Kp indices, and also the IMF Bz index, behave consistently with Dst, and our

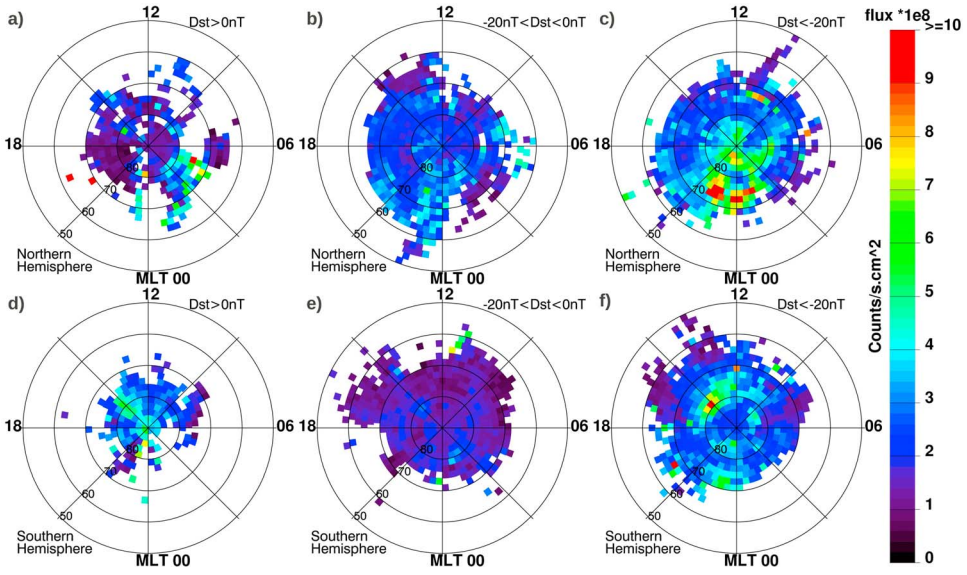

Figure 3. Maps of the source regions for cold ion outflow. Color indicates flux values. (a–c) Average ionospheric outflow fluxes in the northern hemisphere for quiet, moderate and disturbed geomagnetic conditions. (d–f) Corresponding fluxes for southern hemisphere. Each pixel represents the mean flux calculated from at least 5 values, though most pixels are based on 30 values or more.

Table 1. Averages From the *Engwall et al.* [2009b] Data Set for Three Different Geomagnetic Activity Levels for the Northern and Southern Hemispheres

	Activity[a]	AE (nT)	Dst (nT)	Kp	Bx (nT)	By (nT)	Bz (nT)	n_{SW} (cm^{-3})	V_{SW} ($km \cdot s^{-1}$)	F10.7 (10^{-22} $W \cdot s \cdot m^{-2}$)	Pdyn (nPa)	Outflow Area[b] (km^2)	Outflow Rate[c] (s^{-1})
Northern Hemisphere	Quiet	125.4	6.9	1.5	2.4	−2.5	0.4	9.9	396.5	139.9	2.9	1.6×10^7	3.2×10^{25}
	Moderate	200.0	−11.0	2.2	1.1	−1.2	−0.1	5.3	426.4	160.1	1.8	2.8×10^7	6.8×10^{25}
	Disturbed	448.8	−41.6	3.5	−0.7	2.1	−1.4	5.6	470.8	183.7	2.4	2.9×10^7	9.5×10^{25}
Southern Hemisphere	Quiet	196.0	3.2	1.9	−0.2	0.5	0.9	7.9	399.1	165.2	2.4	0.9×10^7	2.5×10^{25}
	Moderate	200.5	−10.6	1.8	0.4	−0.3	−0.5	4.7	436.2	139.6	1.6	2.6×10^7	3.8×10^{25}
	Disturbed	386.3	−43.2	3.0	−1.3	−0.8	−1.0	5.8	445.2	175.1	2.2	2.8×10^7	7.6×10^{25}

[a]Quiet = Dst above 0 nT, Moderate = Dst between −20 nT and 0 nT, Disturbed = Dst below −20 nT.
[b]Sum of area of all colored pixels in Figure 3.
[c]Sum of average fluxes of all colored pixels in Figure 3.

results would not have been fundamentally different if we had chosen any of these parameters as a proxy for geomagnetic activity.

[22] Disturbed periods are typically associated with a southward directed IMF, enhanced magnetospheric convection and enhanced transfer of energy and momentum from the solar wind to the magnetosphere. Conversely, quiet magnetospheric periods are usually associated with a northward directed IMF and stagnant magnetospheric convection. To ensure sufficient statistics, we have classified periods with positive Dst values as geomagnetically quiet, Dst values below −20 nT as disturbed, and anything in between as moderate.

[23] Two distinct properties of the source region are immediately apparent from Figure 3. First, the source area is much larger for moderate and disturbed conditions than for quiet conditions. Second, during disturbed conditions (Figures 3c and 3f), two distinct regions of higher fluxes emerge in the northern and southern hemisphere, respectively. Below, we discuss these results in some detail.

4.1. Size of the Source Area

[24] The polar cap size, i.e., the region of open magnetic flux is known to change with changing energy input from the solar wind, in particular the orientation of the IMF. In general, a southward directed IMF will enhance the dayside reconnection and open more flux - as a consequence, the polar cap region will expand to lower latitudes [e.g., *Sotirelis et al.*, 1998]. Likewise, a northward directed IMF will lead to a contraction of the polar cap region. For extended periods with a strong northward IMF, there are even indications that the polar cap disappears almost completely [*Zhang et al.*, 2009].

[25] Figure 3 suggests a source area centered within the polar cap around 75° latitude for quiet conditions, and a larger source region, expanding equatorward of 70° latitude for moderate and disturbed conditions. In their calculation of the total cold outflow, *Engwall et al.* [2009b, 2009a] assumed a fixed polar cap boundary located at 70° magnetic latitude. From the above results, their choice seems to be reasonable, although perhaps not representative for very quiet magnetospheric conditions.

[26] Table 1 (next to last column) shows the calculated sizes of the source area for each panel of Figure 3. This area is obtained by integrating the areas of the colored pixels in the figure. For the northern hemisphere, the area of the source region increases by almost a factor of 2, and the total outflow rate (Table 1, last column) increases by a factor of 3 between quiet and disturbed conditions (the areas of outflow region during quiet times may be underestimated due to lack of data coverage in the post midnight sector, though). The outflow rates seem to be slightly lower in the southern hemisphere. One plausible explanation for this asymmetry is that the data set is slightly shifted towards southern hemisphere winter conditions (and thus less sunlight and ionization).

[27] The fact that the expansion and contraction of the polar cap are reproduced by our results, suggests that the cold ions observed by Cluster primarily emanate from the polar cap regions. By contrast, *Lockwood et al.* [1985], studying outflow of O^+, found the cusp/cleft area to be the most pronounced source region. Other studies, [e.g., *Yau and André* 1997, Table I] suggest that the auroral region has the largest outflow rates for both H^+ and O^+.

4.2. Morphology of the Outflow

[28] Without any detailed knowledge about the source region, *Engwall et al.* [2009b, 2009a] assumed a homogeneous source when they calculated their total outflow rates. From Figures 3c and 3f, showing source maps for disturbed conditions, we clearly see structures in the source region.

[29] In the northern hemisphere (Figure 3c), we observe a higher fluxes in the midnight sector, with peak around 72°, a region where one would expect some auroral activity. The observed elevated nightside fluxes seem to co-locate with large scale features seen in synoptic maps of average auroral luminosity presented, e.g. in *Liou et al.* [2001]. The peak fluxes are almost an order of magnitude higher than the more homogeneous regions on the dayside and central polar cap. Auroral precipitation is known to enhance ionization, and may lead to a higher production also of cold ions. Alternatively, auroral activity may favor the mechanisms enabling the cold ions to escape. This region of elevated flux near the auroral zone is less pronounced in the southern hemisphere.

[30] In the southern hemisphere, we observe a similar distinct region of elevated fluxes near the expected cusp/cleft region [e.g., *Chen et al.*, 1998]. A similar, but smaller and less pronounced region of elevated fluxes is also apparent in the northern hemisphere around 72–74° latitude. This is a region in which plasma from the Sun can have direct access to the upper atmosphere, and is thus normally associated with ions of higher energies and temperatures than the cold plasma discussed here. The enhanced flux of cold ions can probably be explained by mechanisms similar to those in the auroral zone.

[31] The apparent north–south asymmetry in Figure 3 can partly be attributed to the spacecraft orbit: During disturbed conditions, the ions, in particular from the nightside, will be transported faster downtail and not always reach the

spacecraft altitude. Since observations are on average taken 2 Re higher above the southern hemisphere polar cap, the auroral zone is less pronounced in this hemisphere. Conversely, ions emanating from the dayside will travel to higher altitudes before being convected downtail. Dayside structures are therefore more distinct in the southern hemisphere.

5. Summary

[32] We have used a comprehensive set of measurements from the high altitude polar cap and lobe regions to study the outflow of cold ions from the ionosphere. The measurements cover ion energies up to approximately 70 eV, and are obtained from 5 years of Cluster observations. The data set spans a wide range of solar wind conditions and allows for sorting into subsets.

[33] By tracing the observations down to the topside ionosphere, we have been able to generate maps of the source regions for different geomagnetic activity levels. The main results can be summarized as follows:

[34] 1. For quiet and moderate magnetospheric conditions, the primary source of the cold ions observed by Cluster in the magnetotail seems to be the polar cap regions rather than the auroral zone or cusp/cleft areas.

[35] 2. During disturbed magnetospheric conditions, we observe elevated fluxes near the nightside auroral region and dayside cusp region. This suggests enhanced ionization and/or a more effective transport of cold ions from these regions during active periods.

[36] 3. The size of the source region varies with geomagnetic activity. During geomagnetic quiet conditions, the size of the source is 2–3 times smaller than for intermediate or disturbed conditions. This behavior is consistent with polar cap expansion and contraction, and suggests that the polar cap region is the primary source for the cold ion outflow.

[37] 4. The total outflow rate from each hemisphere varies by a factor 3 with geomagnetic activity level, with outflow rates up to 1×10^{26} ions/s for disturbed conditions.

[38] **Acknowledgments.** The Editor thanks William Lotko and Andrew Howarth for their assistance in evaluating this paper.

References

André, M., and C. M. Cully (2012), Low-energy ions: A previously hidden solar system particle population, *Geophys. Res. Lett.*, *39*, L03101, doi:10.1029/2011GL050242.

Baker, K. B., and S. Wing (1989), A new magnetic coordinate system for conjugate studies at high latitudes, *J. Geophys. Res.*, *94*, 9139–9143, doi:10.1029/JA094iA07p09139.

Balogh, A., et al. (1997), The Cluster Magnetic Field Investigation, *Space Sci. Rev.*, *79*, 65–91.

Chappell, C. R., T. E. Moore, and J. H. Waite Jr. (1987), The ionosphere as a fully adequate source of plasma for the Earth's magnetosphere, *J. Geophys. Res.*, *92*, 5896–5910, doi:10.1029/JA092iA06p05896.

Chen, J., T. A. Fritz, R. B. Sheldon, H. E. Spence, W. N. Spjeldvik, J. F. Fennell, S. Livi, C. T. Russell, J. S. Pickett, and D. A. Gurnett (1998), Cusp energetic particle events: Implications for a major acceleration region of the magnetosphere, *J. Geophys. Res.*, *103*, 69–78, doi:10.1029/97JA02246.

Cladis, J. B. (1986), Parallel acceleration and transport of ions from polar ionosphere to plasma sheet, *Geophys. Res. Lett.*, *13*, 893–896, doi:10.1029/GL013i009p00893.

Dubinin, E., M. Fränz, A. Fedorov, R. Lundin, N. Edberg, F. Duru, and O. Vaisberg (2011), Ion energization and escape on Mars and Venus, *Space Sci. Rev.*, *162*(1–4), 173–211.

Engwall, E., A. I. Eriksson, C. M. Cully, M. André, P. A. Puhl-Quinn, H. Vaith, and R. Torbert (2009a), Survey of cold ionospheric outflows in the magnetotail, *Ann. Geophys.*, *27*, 3185–3201.

Engwall, E., A. I. Eriksson, C. M. Cully, M. André, R. Torbert, and H. Vaith (2009b), Earth's ionospheric outflow dominated by hidden cold plasma, *Nat. Geosci.*, *2*, 24–27, doi:10.1038/NGEO387.

Eriksson, A. I., et al. (2006), Electric field measurements on Cluster: Comparing the double-probe and electron drift techniques, *Ann. Geophys.*, *24*, 275–289, doi:10.5194/angeo-24-275-2006.

Förster, M., G. Paschmann, S. E. Haaland, J. M. Quinn, R. B. Torbert, H. Vaith, and C. A. Kletzing (2007), High-latitude plasma convection form cluster EDI: Variances and solar wind correlation, *Ann. Geophys.*, *25*, 1691–1707.

Gustafsson, G., et al. (2001), First results of electric field and density measurements by Cluster EFW based on initial months of operation, *Ann. Geophys.*, *19*, 1219–1240.

Haaland, S., G. Paschmann, M. Förster, J. Quinn, R. Torbert, H. Vaith, P. Puhl-Quinn, and C. Kletzing (2008), Plasma convection in the magnetotail lobes: Statistical results from Cluster EDI measurements, *Ann. Geophys.*, *26*, 2371–2382.

Haaland, S., et al. (2012), Estimating the capture and loss of cold plasma from ionospheric outflow, *J. Geophys. Res.*, *117*, A07311, doi:10.1029/2012JA017679.

Liou, K., P. T. Newell, and C.-I. Meng (2001), Seasonal effects on auroral particle acceleration and precipitation, *J. Geophys. Res.*, *106*, 5531–5542, doi:10.1029/1999JA000391.

Lockwood, M., J. H. Waite Jr., T. E. Moore, C. R. Chappell, and M. O. Chandler (1985), The cleft ion fountain, *J. Geophys. Res.*, *90*, 9736–9748, doi:10.1029/JA090iA10p09736.

Lybekk, B., A. Pedersen, S. Haaland, K. Svenes, A. N. Fazakerley, A. Masson, M. G. G. T. Taylor, and J.-G. Trotignon (2012), Solar cycle variations of the Cluster spacecraft potential and its use for electron density estimations, *J. Geophys. Res.*, *117*, A01217, doi:10.1029/2011JA016969.

Moore, T. E., and J. L. Horwitz (2007), Stellar ablation of planetary atmospheres, *Rev. Geophys.*, *45*, RG3002, doi:10.1029/2005RG000194.

Nilsson, H., E. Engwall, A. Eriksson, P. A. Puhl-Quinn, and S. Arvelius (2010), Centrifugal acceleration in the magnetotail lobes, *Ann. Geophys.*, *28*, 569–576.

Northrop, T. G. (1963), *The Adiabatic Motion of Charged Particles*, John Wiley, New York.

Paschmann, G., et al. (2001), The Electron Drift Instrument on Cluster: Overview of first results, *Ann. Geophys.*, *19*, 1273–1288.

Pedersen, A., et al. (2001), Four-point high time resolution information on electron densities by the electric field experiments (EFW) on Cluster, *Ann. Geophys.*, *19*, 1483–1489, doi:10.5194/angeo-19-1483-2001.

Peterson, W. K., H. L. Collin, O. W. Lennartsson, and A. W. Yau (2006), Quiet time solar illumination effects on the fluxes and characteristic energies of ionospheric outflow, *J. Geophys. Res.*, *111*, A11S05, doi:10.1029/2005JA011596.

Seki, K., et al. (2003), Cold ions in the hot plasma sheet of Earth's magnetotail, *Nature*, *422*, 589–592.

Sotirelis, T., P. T. Newell, and C. Meng (1998), Shape of the open-closed boundary of the polar cap as determined from observations of precipitating particles by up to four DMSP satellites, *J. Geophys. Res.*, *103*, 399–406, doi:10.1029/97JA02437.

Tsyganenko, N. A., and M. I. Sitnov (2005), Modeling the dynamics of the inner magnetosphere during strong geomagnetic storms, *J. Geophys. Res.*, *110*, A03208, doi:10.1029/2004JA010798.

Wei, Y., et al. (2012), Enhanced atmospheric oxygen outflow on Earth and Mars driven by a corotating interaction region, *J. Geophys. Res.*, *117*, A03208, doi:10.1029/2011JA017340.

Yau, A. W., and M. André (1997), Sources of ion outflow in the high latitude ionosphere, *Space Sci. Rev.*, *80*, 1–25, doi:10.1023/A:1004947203046.

Zhang, Y., L. J. Paxton, P. T. Newell, and C.-I. Meng (2009), Does the polar cap disappear under an extended strong northward IMF?, *J. Atmos. Sol. Terr. Phys.*, *71*(17–18), 2006–2012, doi:10.1016/j.jastp.2009.09.005.